Bulletin of the Seismological Society of America, Vol. 107, No. 1, pp. 132–148, February 2017, doi: 10.1785/0120160208

Adjusting Central and Eastern North America Ground-Motion Intensity Measures between Sites with Different Reference-Rock Site Conditions

by David M. Boore and Kenneth W. Campbell

Abstract Adjustment factors are provided for converting ground-motion intensity measures between central and eastern North America (CENA) sites with different reference-rock site conditions (V_{S30} = 760, 2000, and 3000 m/s) for moment magnitudes ranging from 2 to 8, rupture distances ranging from 2 to 1200 km, Fourier amplitude spectra (FAS) for frequencies ranging from 0.01 to 100 Hz, response spectra for periods ranging from 0.01 to 10.0 s, peak ground acceleration, and peak ground velocity. The adjustment factors are given for a wide range of the site diminution parameters (κ_0) for sites with V_{S30} = 760 m/s and for a κ_0 of 0.006 s for two harder rock sites. Fourteen CENA velocity profiles with V_{S30} values within a factor of 1.1 of 760 m/s were used to derive average FAS amplification factors as a function of frequency, which were then used in simulations of peak ground-motion parameters and response spectra to derive the adjustment factors. The amplification function differs from that used in western North America (e.g., Campbell and Boore, 2016) in having a peak near 9 Hz, due to the resonance of motions in the relatively thin low-velocity material over hard rock that characterizes many CENA sites with V_{S30} near 760 m/s. We call these B/C sites, because this velocity marks the boundary between National Earthquake Hazards Reduction Program site classes B and C (Building Seismic Safety Council, 2004). The adjustments for short-period motions are sensitive to the value of κ_0, but there are very few if any determinations of κ_0 for CENA B/C sites. For this reason, we determined κ_0 from multiple recordings at Pinyon Flat Observatory (PFO), California, which has a velocity-depth profile similar to those of CENA B/C sites. The PFO and other results from the literature suggest that appropriate values of κ_0 for CENA B/C sites are expected to lie between 0.01 and 0.03 s.

Electronic Supplement: Zip files with parameters used by Stochastic-Method SIMulation (SMSIM) and ratios of the ground-motion intensity measures between hard-rock sites and National Earthquake Hazards Reduction Program (NEHRP) B/C sites.

Introduction

Ground-motion prediction equations (GMPEs) in central and eastern North America (CENA) are usually for hard-rock (HR) sites, defined herein as sites with V_{S30} in the 1500–2000 m/s range, but the need often arises to evaluate motions for sites characterized by V_{S30} different than that used in developing the GMPEs. An example is in the development of the U.S. Geological Survey's (USGS) National Seismic Hazard Model (NSHM; Frankel *et al.*, 1996, 2002; Petersen *et al.*, 2008, 2014), for which the motions are for a B/C site (V_{S30} = 760 m/s), but most of the GMPEs used to develop the model were for much harder sites. Adjustments are also sometimes needed to convert motions on softer materials to those on harder sites. Examples of this need arose in the Next Generation Attenuation-East (NGA-East) project (Pacific Earthquake Engineering Research Center [PEER], 2015), in which the specified site condition for the ground-motion models from the developer teams was a reference-rock site with V_{S30} = 3000 m/s and κ_0 = 0.006 s as defined by Campbell *et al.* (2014), Hashash, Kottke, Stewart, Campbell, Kim, Rathje, and Silva (2014), and Hashash, Kottke, Stewart, Campbell, Kim, Moss, *et al.* (2014). However, the ground-motion intensity measures (IMs) used directly in developing empirically based ground-motion models and also used as a check on simulation-based models were all from sites with much smaller values of V_{S30}. This is shown in Figure 1, which displays the distribution of V_{S30} values for

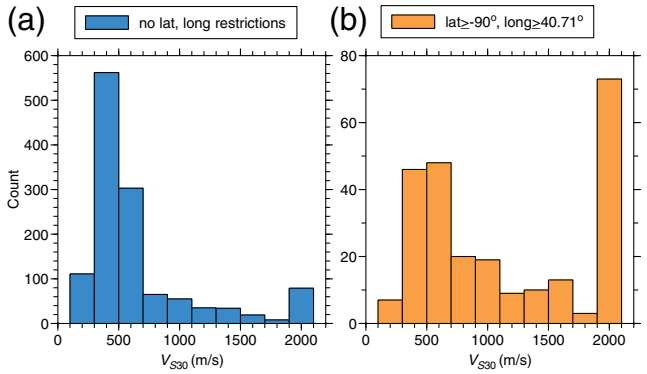

Figure 1. Histograms of V_{S30} values in the 18 November 2014 version of the Next Generation Attenuation-East (NGA-East) flatfile (Goulet *et al.*, 2014). (a) All sites; (b) the subset of sites east of St. Louis, Missouri, and north of New York City, New York (an approximate way of choosing sites in the northeastern United States and southeastern Canada). The color version of this figure is available only in the electronic edition.

CENA (see Data and Resources for source of the V_{S30} values). The figure is composed of two parts: the left graph shows the distribution for all sites, and the right graph shows the distribution for sites somewhat subjectively defined as being in southeastern Canada and northeastern United States (north of New York City, New York, and east of St. Louis, Missouri), for which we expect generally high values of V_{S30} due to the Pleistocene glaciations that removed the softer near-surface rock, leaving behind various thicknesses of glacial deposits. It is clear that most of the sites in the NGA-East database (Goulet *et al.*, 2014) correspond to stiff-soil and soft-rock conditions ($V_{S30} < 760$ m/s). The distribution of V_{S30} in southeastern Canada and northeastern United States is quite different, however, with a number of sites corresponding to HR site conditions. Although most, if not all, of the $V_{S30} = 2000$ m/s assignments shown in Figure 1 are estimated from information such as local site geology, topographic slope, or type of terrain (Goulet *et al.*, 2014) and are not based on measurements, the value of $V_{S30} = 2000$ m/s serves as a proxy for sites that likely would be classified as being HR if measured shear-wave profiles were available at the sites.

The site adjustments proposed in this study are developed for four types of IMs: 5% damped pseudoabsolute response spectral acceleration (PSA), peak ground velocity (PGV), peak ground acceleration (PGA), and Fourier amplitude spectra (FAS). The need for the first three has existed for many years (e.g., in the various editions of the NSHMs), but the need to adjust FAS has arisen relatively recently, at least in the context of specifying the more traditional IMs used by engineers (PSA, PGA, and PGV). For example, Hollenback *et al.* (2015) adjust observed FAS to an HR reference-rock site condition of $V_{S30} = 3000$ m/s using the adjustment factors given in Boore (2015a), and then they use regression analysis to develop equations for specifying FAS in terms of various predictor variables, including local site conditions. Following the pioneering work of Bora *et al.* (2014, 2015), Hollenback *et al.* (2015) use random-vibration theory together with a duration model to predict the more traditional IMs.

The method for adjusting observed or predicted motions between various site conditions is relatively straightforward. For FAS, the adjustments are simply the ratios of the crustal amplifications for the different site conditions, because this ratio does not depend on magnitude or distance if the site response is linear, as assumed. The process is somewhat more complicated for PSA, PGA, and PGV, as these IMs require simulations of motions, which are a function of magnitude and distance. This latter approach has been used by several CENA GMPE developers (e.g., Frankel *et al.*, 1996; Campbell, 2003, 2004; Atkinson and Boore, 2006, 2007; Boore, 2015a,b; Pezeshk *et al.*, 2015). The approach is summarized as follows:

1. Adjust observed IMs to an intermediate reference site condition (usually $V_{S30} = 760$ m/s) using a site term similar to that used in GMPEs. The site term most commonly used is of the form $\ln \mathrm{IM} \approx c \ln(V_{S30}/V_{\mathrm{REF}})$, in which the coefficient c could be derived by one of the following approaches: (a) using the site terms developed for other regions (e.g., Seyhan and Stewart, 2014, for ground motions from earthquakes in active crustal regions) directly, as was done in the development or calibration of several of the NGA-East GMPEs (Hassani and Atkinson, 2015; Pezeshk *et al.*, 2015; Shahjouei and Pezeshk, 2015; Yenier and Atkinson, 2015a); this assumes that stiff-soil and soft-rock site responses are similar in CENA and western North America (WNA), (b) using site-response simulations to develop CENA-specific amplification factors (Harmon, 2016; Harmon *et al.*, 2016), or (c) using empirical site factors developed directly from CENA recordings, with additional input from simulations as needed (Parker *et al.*, 2016).
2. Simulate IMs for many magnitudes (**M**), distances (R_{RUP}, the closest distance to the rupture surface), and oscillator periods (T) for the FAS crustal amplifications corresponding to the reference site and the site of interest.
3. Form the ratios of the IMs for the two sets of amplifications. These ratios are the second set of adjustment factors to be applied to the motions, the first set being from step 1. As will be shown in later sections of this article, the adjustment ratios are relatively constant for ranges of **M**, R_{RUP}, and T important to engineering applications; therefore, simple ratios of the FAS amplifications can be used for the adjustments.

In this article, we first provide crustal amplifications for FAS for V_{S30} values of 760, 2000, and 3000 m/s. We spend considerable effort in defining the crustal amplification for an average B/C site, with $V_{S30} = 760$ m/s, based on 14 shear-wave velocity (V_S) profiles that are either measured or derived from measurements. As the amplifications for HR sites are relatively small and are not sensitive to the specific velocity models, we devote little discussion to these, deferring instead to results of Boore and Thompson (2015) and Boore (2015a).

Table 1
Shear-Wave Velocity Profiles Used in Computing the Average Crustal Amplification for Eastern North America Sites with V_{S30} = 760 m/s

Profile Name	Location	V_{S30} (m/s)	Z_{max} (m)	Source
BJ97 HR	CENA	2780	8000	Boore and Joyner (1997)
Fea96	CENA	760	8000	Frankel *et al.* (1996)
Appalachians	CENA	3520	39,000	Dreiling *et al.* (2014)
HH1000	CENA	760	30	J. A. Harmon (written comm., 2014)
HH3000	CENA	760	89	J. A. Harmon (written comm., 2014)
BLA	Montgomery County, Virginia	804	46	J. A. Harmon (written comm., 2016)
Clinton	De Witt County, Illinois	717	1859	J. A. Harmon (written comm., 2016
HAIL	Harrisburg, Illinois	765	30	Odum *et al.* (2010), Refraction model
Hatch	Baxley, Georgia	762	122	J. C. Chen (written comm., 1991)
MVMO	St. Louis, Missouri	722	30	Williams *et al.* (2007)
OTT	Ottawa	755	70	Beresnev and Atkinson (1997)
Palisades	Van Buren County, Michigan	819	43	J. A. Harmon (written comm., 2016)
S760C	Catawba Nuclear Station, modified; Rock Hill, South Carolina	762	30	W. Silva (written comm., 2014)
SCMO	St. Louis, Missouri	787	30	Williams *et al.* (2007)
SCOT	St. Louis, Missouri	739	30	Williams *et al.* (2007)
STM	St. Marys, Ontario	834	70	Read *et al.* (2008)
USIN	Evansville, Indiana	707	30	Odum *et al.* (2010)
LNP1	Levy County, Florida	731	1295	J. A. Harmon (written comm., 2016)
PFO	Pinyon Flat, California	758	33	Yong *et al.* (2013)

CENA, central and eastern North America; PFO, Pinyon Flat Observatory

We then present the ratios of the IMs needed for step 3. We finish with a discussion of the diminution parameter κ_0 estimated from recordings at a site in California that has a velocity profile similar to that of a typical CENA B/C site; thus, we propose that this California site can serve as a proxy for a CENA B/C site similar to the suggestions of others (Silva *et al.*, 1999; Campbell, 2009; Campbell *et al.*, 2014).

Average Crustal Amplification for Generic CENA Rock Sites

Velocity Profiles for Sites with V_{S30} near 760 m/s

The FAS amplifications are based on velocity profiles. As profiles for sites with the same or similar V_{S30} can vary, it is important to compute the FAS amplifications for a suite of profiles to capture the variability of the amplifications. In this section, we discuss the V_S profiles used in computing the FAS amplification factors. The compilation, given in Table 1, contains 15 sites for which the shear-wave velocity profiles start at the surface and extend to at least 30 m and for which V_{S30} has values within a factor of 1.1 of 760 m/s (admittedly an arbitrary factor, but the number of resulting models is such that the average amplification should be somewhat insensitive to the particular range of V_{S30} used to populate the set of profiles). The profiles include two provided by Y. Hashash and J. Harmon (written comm., 2014), referred to as HH1000 and HH3000, that are guided by the gradient of velocity versus depth from a number of measured V_S profiles. A third profile (HH2000) provided by these investigators was intermediate between the HH1000 and HH3000 profiles used in this article and was found to be unnecessary for our purposes. The HH profiles have shear-wave velocities of 3000 m/s within about 100 m of the surface. We were initially skeptical that such high velocities could occur at such shallow depths, but a number of the measured profiles that we subsequently collected have velocities close to or greater than 3000 m/s within 50 m of the surface, including those of Beresnev and Atkinson (1997).

The 15 profiles are shown in Figure 2 for two maximum depths to show different details of the profiles. The profiles are shown using both shear-wave velocity and slowness (S_S, the inverse of velocity). Slowness is more directly related to the amplification of the incoming waves than is velocity and, as can be seen in Figure 2, plots of slowness emphasize the variations in material properties near the surface (e.g., Brown *et al.*, 2002; Boore and Thompson, 2007). The figure legends contain important information about the profiles, such as the location of the site and the source and maximum depth of the profiles. The profiles have been extended to greater depths than the maximum depths of each original profile by merging them with one of three deeper profiles given by Frankel *et al.* (1996; hereafter, Fea96), Boore and Joyner (1997; hereafter, BJ97 HR), and Dreiling *et al.* (2014; hereafter, Appalachians) as shown in Figure 2. Due to their similarity, only one of the three Dreiling *et al.* (2014) profiles is shown. The Dreiling *et al.* (2014) profiles did not attempt to capture near-surface velocities, but they are useful as a way of judging the appropriateness of using the BJ97 HR and Fea96 profiles for extending the shallower profiles to greater depths. The BJ97 HR and Dreiling *et al.* (2014) profiles are similar; in contrast, Fea96, which was modified from a WNA profile, has higher slownesses at depth than either of the other two profiles and might not be appropriate for CENA.

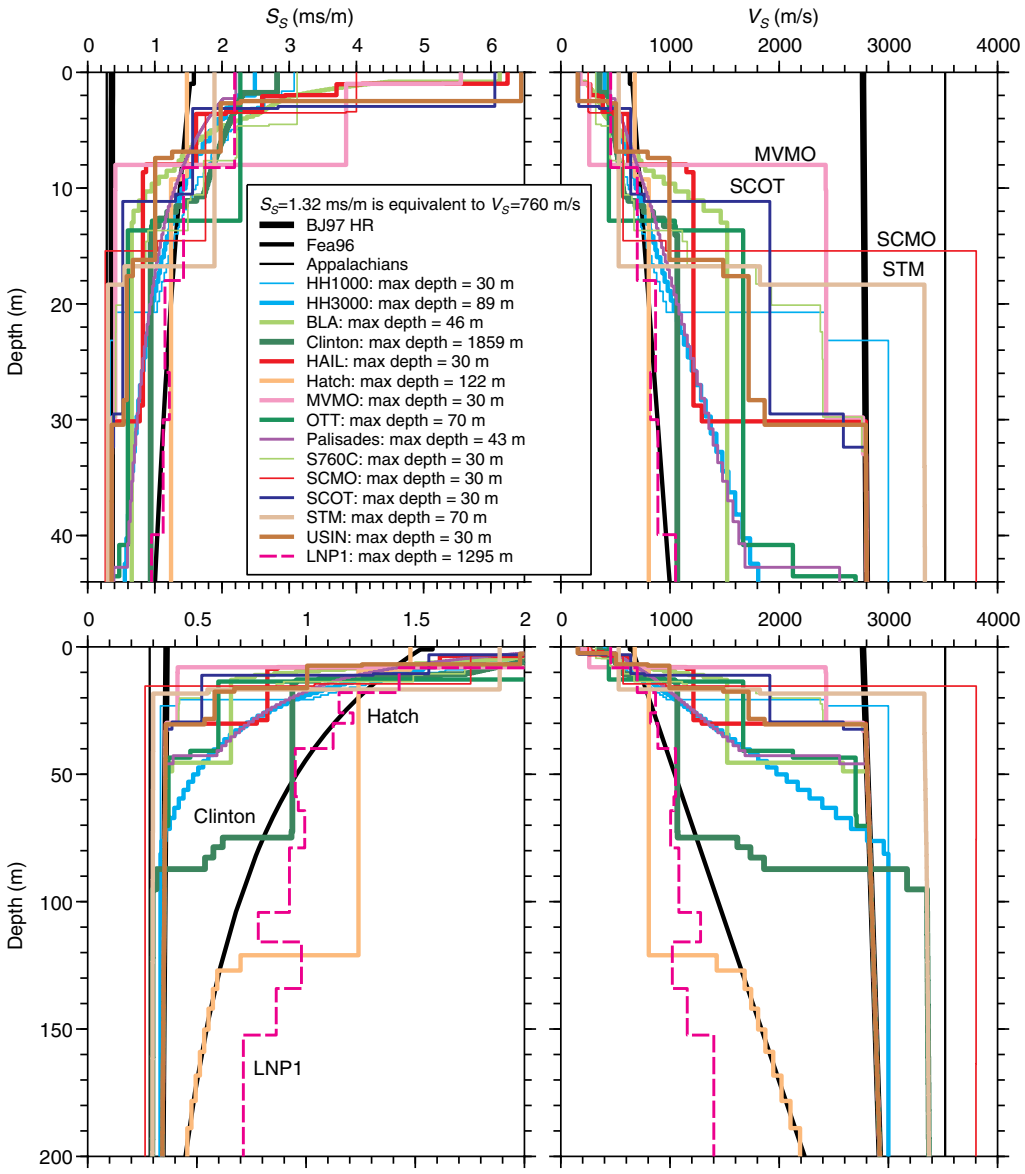

Figure 2. Shear-wave slowness (S_S) and velocity (V_S) versus depth for 15 extended profiles with V_{S30} within a factor of 1.1 of 760 m/s. Several deeper profiles are also included (Frankel *et al.*, 1996; hereafter, Fea96; Boore and Joyner, 1997; hereafter BJ97 HR; and Dreiling *et al.*, 2014; hereafter Appalachians), which were used to extend the shallow profiles to 8 km. LNP1 was excluded from the calculations of average amplifications (see the Velocity Profiles for Sites with V_{S30} near 760 m/s section). See Table 1 for more information about the profiles. The maximum depths of 44 and 200 m were chosen to reveal near-surface and deeper details, respectively. The color version of this figure is available only in the electronic edition.

We do not intend the reader to differentiate between the slowness profiles shown in Figure 2, but rather we present them to provide an overall impression of the similarities between the profiles. In general, the profiles are characterized by relatively thin low-velocity (high-slowness) layers overlying much harder (low-slowness) materials. As shown in the next section, this large change in slowness over a small range of depths leads to pronounced resonances in the site response. In the lower row of Figure 2, we labeled three of the profiles (Clinton, Hatch, and LNP1), because they differ rather significantly from the other profiles. The large impedance change in the Clinton profile is part of the original profile, while that for Hatch is a direct result of merging that profile with the Fea96 profile. In both cases, the large impedance change over a shorter depth range leads to resonant amplifications at lower frequencies than that exhibited by the other profiles (as shown later). The LNP1 profile, which is anomalous relative to all of the other profiles, is from Florida, and we discard it as not being representative of the CENA sites of interest in this study. We are left with 14 profiles that were use to derive average site amplifications for a B/C site in CENA. It is tempting to classify these sites as glaciated,

because such sites are often thought of as having a thin layer of softer materials over HR at shallow depths. However, that would be an oversimplification. For example, sites MVMO, SCMO, and SCOT shown in the right, upper graph of Figure 2 are from the St. Louis, Missouri, area. A careful comparison of the locations of these sites (as shown in fig. 2 of Williams *et al.*, 2007) with the southern extent of Pleistocene glaciations shown in figure 43.1 of Rovey and Balco (2011) shows that these sites are likely to be just south of the glaciated region. In this case, the transition to HR at shallow depths is because the sites have a thin (generally 6–30 m) cover of Quaternary (sediments) overlying Paleozoic carbonate rocks (Williams *et al.*, 2007). It could be that there are other B/C sites in CENA for which there is not a transition to HR at relatively shallow depths (e.g., LNP1, mentioned previously). For such sites, the B/C amplifications would be different than the average amplifications developed in this article, and therefore there would be a regional dependence to the B/C-to-HR adjustment factors. We have no basis for determining the amplifications for these other types of B/C sites at this time; accordingly, our results are only for B/C sites characterized by a transition over a limited range of depths to HR at relatively shallow depths. We refer to such sites as generic CENA B/C sites, with the understanding that other B/C sites with more slowly increasing velocity with depth might exist in CENA, as characterized by Campbell (2009).

Crustal Amplification for a Generic CENA B/C Site

We use the velocity profiles discussed above to generate crustal amplifications, which are then used in the simulations to derive the adjustment ratios. In previous studies of generic amplification models (e.g., Boore and Joyner, 1997; Boore and Thompson, 2015; Campbell and Boore, 2016), the amplifications are computed using the square-root-impedance (SRI) method most recently described in Boore (2013). The SRI amplifications are smooth functions of frequency and always underestimate the fundamental-mode resonant peak. On the other hand, the SRI amplifications are close to the root mean square of the full-resonant amplifications when averaged over many higher modes (Boore, 2013). Because the intent in this study, as in previous ones, is to derive an average amplification for a generic site, the rationale for using SRI amplifications is the assumption that the frequencies of the resonant peaks shift from site to site in such a way that the resonant peaks at any one site would be smoothed out when averaged over many sites, making the SRI amplifications (which are very simple and rapid to compute) appropriate for defining an average amplification model. The similarity of the slowness models shown in Figure 2 suggests that this might not be the case for typical B/C sites in CENA. For that reason, we also used full-resonant amplifications as shown in Figure 3 to inform our average amplification model. All amplifications assume linear response and are relative to the motions on a fictitious rock outcrop underlain by a uniform material with a density and V_S of 2.8 g/cm^3 and

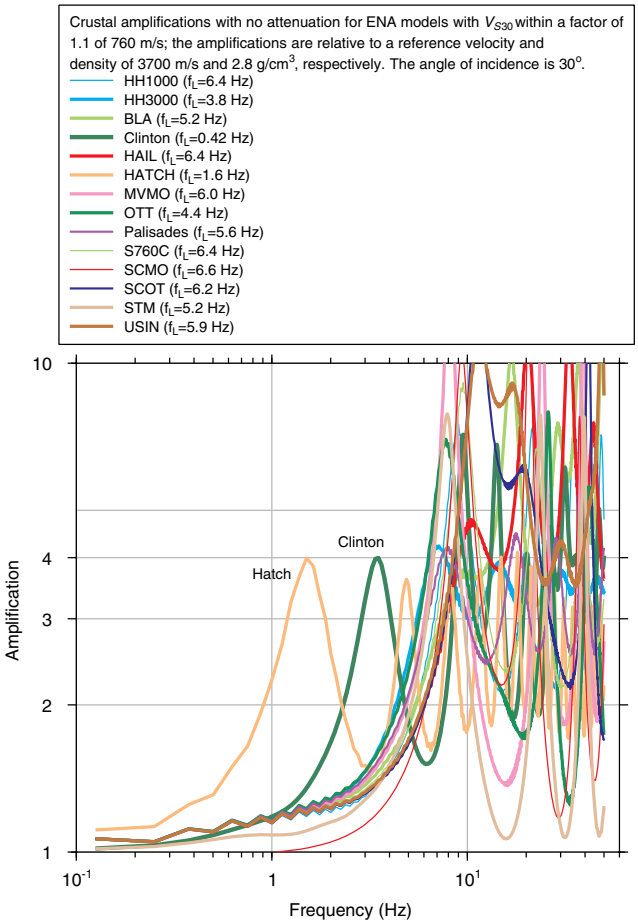

Figure 3. Full-resonant crustal amplifications for 14 extended profiles with V_{S30} within a factor of 1.1 of 760 m/s, assuming plane horizontally polarized shear waves with a 30° angle of incidence at a depth of 8 km. The amplifications are relative to the motion at an equivalent surface outcrop underlain by a uniform material with a V_S and density of 3700 m/s and 2.8 g/cm^3, respectively. f_L is the frequency for which a quarter-wavelength equals the maximum depth of the original, unextended profiles. The color version of this figure is available only in the electronic edition.

3.7 km/s, respectively. The simulations are for plane horizontally polarized shear waves with a 30° angle of incidence at a depth of 8 km. The choice of this angle of incidence is discussed in Boore (2013); the results are almost the same when a 0° angle of incidence is used. There is no attenuation in the amplification models. We show in the legend to Figure 3 the frequency (f_L) for which a quarter-wavelength corresponds to the maximum depth of each original profile before extending the profile to greater depths. This quantity is useful in assessing the frequency ranges associated with the amplifications from the original profiles as opposed to the ranges corresponding to the choices we made in extending the profiles to greater depths. As with the slowness and velocity plots, we do not expect the reader to differentiate between the curves. It is sufficient to observe that the first resonant peak of each profile is generally close to 10 Hz and that this frequency is greater than f_L, indicating that it is a

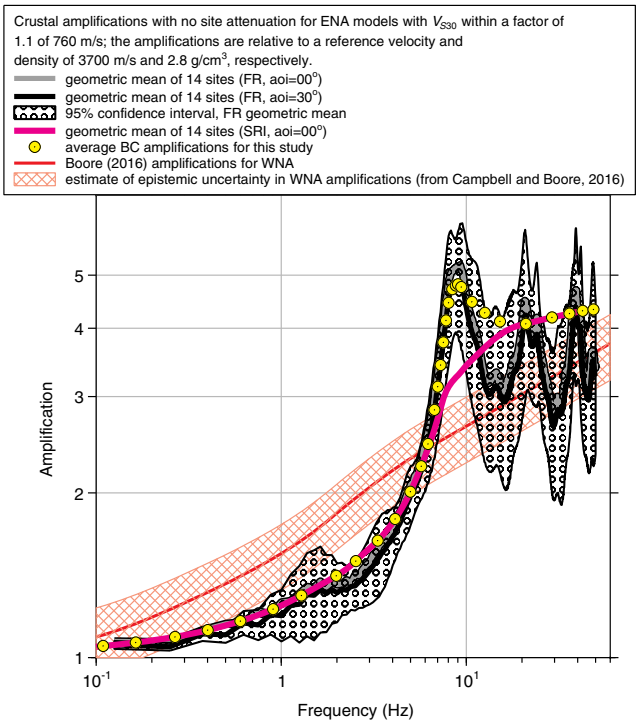

Figure 4. The average amplification (dots) to be used in the adjustments discussed in this article, based on the geometric mean and its 95% confidence limits of the 14 full-resonant amplifications shown in Figure 3 (using an angle of incidence of 30°; for comparison, the geometric mean of amplifications computed using a 0° angle of incidence is also shown) and the geometric mean of the square-root-impedance (SRI) amplifications for the 14 profiles used to compute the full-resonant amplifications. For comparison, the average crustal amplification for a generic western North America (WNA) B/C site from Boore (2016) and the spread of that amplification from Campbell and Boore (2016) is also shown. The color version of this figure is available only in the electronic edition.

property of the profiles themselves and not of the assumed extension of these profiles to greater depths. The exceptions to this are for the Clinton and Hatch sites, for which the resonant frequencies are less than 10 Hz.

The geometric mean of the 14 individual FAS full-resonant amplifications shown in Figure 3, together with the geometric mean of the SRI amplifications for those sites, is shown in Figure 4. Also shown in this figure are the geometric mean for the full-resonant amplification for a 0° angle of incidence and the 95% confidence intervals of the average full-resonant amplification. The full-resonant amplifications are almost the same for both angles of incidence. The average amplification that we propose to be used for a generic CENA B/C site was obtained by a combination of the average full-resonant and the SRI amplifications. A combination was used because we did not want the generic amplification to be strongly influenced by the higher-mode peaks and troughs, but we did want to capture the consistent fundamental resonance near 9 Hz. The generic amplification that we have subjectively chosen is shown by the circles. For comparison, the generic B/C amplification of Boore (2016) for WNA, as discussed in Campbell and Boore (2016), is also shown for comparison in Figure 4. Although both the CENA and WNA amplifications are for a $V_{S30} = 760$ m/s site, we note that the average amplifications are quite different. For frequencies less than about 6 Hz, the CENA amplifications are lower than those for WNA. This is because the velocity increases with depth more rapidly in CENA than in WNA. On the other hand, as discussed previously, the relatively thin low-velocity materials over HR in CENA lead to a strong site resonance near 9 Hz. Because a number of sites in WNA are underlain by materials with a gradient rather than a step-like change in velocity, Boore (2016) chose not to include a resonance effect in his computation of the WNA amplification (see also Boore, 2013). The presence of a resonant peak is a major difference between the generic amplifications that we are proposing for CENA and what Boore (2016) and Campbell and Boore (2016) propose for WNA or, for that matter, what others have proposed for CENA (e.g., Atkinson and Boore, 2006; Yenier and Atkinson, 2015a).

Generic Crustal Amplifications for Hard-Rock Sites

The velocity profiles used for the crustal amplifications for HR sites in CENA are based on the BJ97 HR profile. For an HR site with $V_{S30} = 3000$ m/s, the top 300 m of the BJ97 HR profile was replaced by a layer with a velocity of 3000 m/s as recommended by Boore and Thompson (2015). For an HR site with $V_{S30} = 2000$ m/s, the top 30 m of the profile was assigned a V_S of 2000 m/s and underlain by material with a linear gradient that joins the BJ97 HR profile at a depth of 300 m, as recommended by Boore and Thompson (2015). Plots of these velocity profiles are given in figure 8 of Boore (2015a). The amplifications were computed using the SRI method. We do not provide more detail here because the amplifications are quite small and are insensitive to differences in the HR velocity profiles. The models and amplifications are discussed in greater detail in Boore (2015a).

Comparison of Generic CENA Crustal Amplifications

The FAS crustal amplifications for the three site conditions addressed in this article (V_{S30} of 760, 2000, and 3000 m/s) are compared in Figure 5. The amplifications have no site attenuation applied to them (i.e., $\kappa_0 = 0$ s). When site attenuation is included, it is usually applied directly to the FAS using the diminution operator $\exp(-\pi\kappa_0 f)$, as shown in Figure 5 for a range of κ_0 values. At higher frequencies, the amplifications are controlled by the shallow parts of the velocity profiles, which can have significant variations. Because site attenuation reduces the FAS at high frequencies, short-period PSA will be controlled by lower-frequency ground motions. The consequence is that the variability of the short-period PSA will be less than inferred from the unattenuated FAS amplifications. The reduction of the FAS at high frequency due to site attenuation is illustrated in

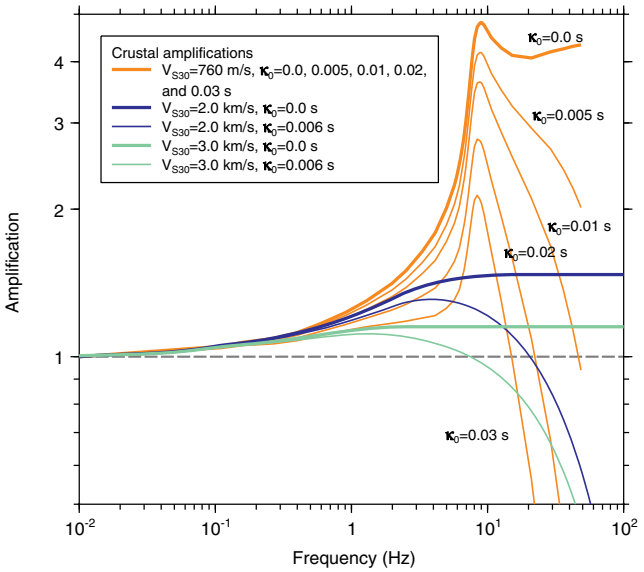

Figure 5. Crustal amplifications of Fourier amplitude spectra (FAS) for three site conditions. The amplifications include the diminution operator $\exp(-\pi\kappa_0 f)$, with a range of κ_0 values. The color version of this figure is available only in the electronic edition.

Figure 5. We used $\kappa_0 = 0.006$ s for the two HR sites, the value chosen for the HR reference site in the NGA-East project (Campbell *et al.*, 2014) and a range of κ_0 values for the generic B/C site. The resultant amplification, including site attenuation, for sites with $V_{S30} = 760$ m/s is larger than that for the higher-velocity sites, except at high frequencies, at which the decrease due to the diminution operators for the lower-velocity site overwhelms the greater unattenuated amplification for that site. This kappa-effect has an impact on the B/C-to-reference rock adjustment factors (defined as the IM for a reference-rock site divided by that for a B/C site), which tend to become greater than unity at short periods as κ_0 increases and **M** decreases, as we show in the next section.

Site Adjustment Factors for Ground-Motion Intensity Measures

The generic crustal amplifications shown in Figure 5 are for FAS. The adjustment factor to convert FAS from a site with $V_{S30} = V_1$ to one with $V_{S30} = V_2$ is simply the ratio of the average amplifications for the two sites. The unattenuated ($\kappa_0 = 0.0$ s) FAS amplifications and their ratios (adjustment factors) for the three values of V_{S30} considered in this article are given in Table 2. The adjustment factors for particular values of κ_0 are obtained by multiplying the values in Table 2 by the diminution operator $\exp(-\pi\Delta\kappa_0 f)$, in which $\Delta\kappa_0$ is the difference of κ_0 at the two sites. Adjustment factors are more complex for the more traditional IMs of PSA, PGA, and PGV that are typically used in engineering. Because these IMs can be controlled by a range of ground-motion frequencies, the adjustment factors can be a function of magnitude and distance. In this article, the magnitude and distances used are moment magnitude (**M**) and rupture distance (R_{RUP}). Because of the possible **M** and R_{RUP} dependence of the adjustment factors, simulations are required, with the adjustment factor (AF) being computed from the ratio of Y for each V_{S30} generic amplification by:

$$\mathrm{AF} = \frac{Y(V_{S30} = V_1)}{Y(V_{S30} = V_2)}, \tag{1}$$

in which Y is a simulated IM for the indicated site condition and for a specified magnitude and distance (this dependence is implied in equation 1, although it is not indicated explicitly). The simulations were done using the stochastic simulation model Stochastic-Method SIMulation (SMSIM; Boore, 2005) with a single-corner-frequency source model. We computed Y using the attenuation model of Boatwright and Seekins (2011; hereafter, BS11), with $1/R^{1.0}$ decay within the first 50 km, followed by a decay of $1/R^{0.5}$. For consistency with the attenuation model, we used a median stress parameter of 172 bars, which was determined by Boore (2015b) by inverting the data of Boore *et al.* (2010) and Boore (2012) using the BS11 attenuation model. As shown in Boore (2015a), the values of AF are not sensitive to the geometric attenuation model that is used in the simulations. The Boore and Thompson (2015) path durations and finite-fault adjustment factors for earthquakes in stable continental regions were used in the computations. All model parameters used in the simulations are contained in the SMSIM parameter files included in the Ⓔ electronic supplement to this article. Also included in the electronic supplement are files containing tables of the adjustment factors. Interpolation of these tables can be used to obtain adjustment factors for nontabulated oscillator periods, magnitudes, and distances.

Representative results for $V_1 = 3000$ m/s and $V_2 = 760$ m/s are shown in Figure 6 as a function of rupture distance (R_{RUP}) for four magnitudes (**M** = 2.0, 4.0, 6.0, and 8.0) and two values of κ_0 (0.01 and 0.03 s), and for PGA, PGV, and six values of PSA ($T = 0.05$, 0.1, 0.2, 0.5, 1, and 2 s). This figure also shows the adjustment factors for FAS at the same frequencies as the PSA oscillator frequencies. No FAS ratios are shown for PGA and PGV, because it is not clear what FAS frequency range should be used for these two IMs.

The inverse of the adjustment factors used in the NSHM to adjust IMs from CENA GMPEs developed for HR to a B/C site condition is also shown in Figure 6 (e.g., Frankel *et al.*, 1996, 2002; Petersen *et al.*, 2008, 2014; these authors did not provide an adjustment factor for $T = 0.05$ s). The distance range shown for the NSHM adjustments (out to 50 km) is the one considered by the NHSM program in choosing a distance-independent adjustment factor. The NSHM adjustments used $\kappa_0 = 0.01$ s with FAS adjustment factors derived using the V_S profile of Fea96. Generally, the NSHM HR to B/C adjustments are similar to ours for $\kappa_0 = 0.01$ s, but the peak near 10 Hz in our B/C amplification, which was not present in the amplification used in deriving the NSHM adjustments, reduces our adjustment

Table 2

Unattenuated ($\kappa_0 = 0.0$ s) Fourier amplitude spectra (FAS) Crustal Amplification Factors and Amplification Ratios for a Generic CENA B/C Site and for Generic CENA Hard-Rock Sites with $V_{S30} = 2000$ and 3000 m/s

f*	A_{760}*	A_{2000}	A_{3000}	A_{3000}/A_{760}	A_{3000}/A_{2000}	A_{760}/A_{3000}	A_{2000}/A_{3000}
0.01	1.000	1.000	1.005	1.00	1.00	1.00	1.00
0.11	1.050	1.055	1.048	1.00	0.99	1.00	1.01
0.16	1.064	1.067	1.058	0.99	0.99	1.01	1.01
0.27	1.092	1.092	1.075	0.98	0.98	1.02	1.02
0.40	1.122	1.119	1.091	0.97	0.97	1.03	1.03
0.60	1.166	1.153	1.108	0.95	0.96	1.05	1.04
0.90	1.226	1.196	1.126	0.92	0.94	1.09	1.06
1.29	1.299	1.244	1.141	0.88	0.92	1.14	1.09
1.98	1.410	1.312	1.150	0.82	0.88	1.23	1.14
2.53	1.501	1.354	1.151	0.77	0.85	1.30	1.18
3.32	1.636	1.391	1.151	0.70	0.83	1.42	1.21
4.13	1.793	1.415	1.151	0.64	0.81	1.56	1.23
4.99	2.010	1.430	1.151	0.57	0.80	1.75	1.24
5.71	2.236	1.440	1.151	0.51	0.80	1.94	1.25
6.21	2.458	1.446	1.151	0.47	0.80	2.14	1.26
6.73	2.836	1.449	1.151	0.41	0.79	2.46	1.26
7.02	3.130	1.451	1.151	0.37	0.79	2.72	1.26
7.27	3.428	1.453	1.151	0.34	0.79	2.98	1.26
7.52	3.770	1.454	1.151	0.31	0.79	3.28	1.26
7.77	4.133	1.456	1.151	0.28	0.79	3.59	1.26
8.02	4.452	1.457	1.151	0.26	0.79	3.87	1.27
8.40	4.714	1.460	1.151	0.24	0.79	4.10	1.27
8.77	4.787	1.461	1.151	0.24	0.79	4.16	1.27
9.02	4.811	1.462	1.151	0.24	0.79	4.18	1.27
9.40	4.756	1.463	1.151	0.24	0.79	4.13	1.27
10.72	4.470	1.466	1.151	0.26	0.79	3.88	1.27
12.60	4.268	1.469	1.151	0.27	0.78	3.71	1.28
15.20	4.116	1.471	1.151	0.28	0.78	3.58	1.28
20.99	4.074	1.471	1.151	0.28	0.78	3.54	1.28
29.07	4.185	1.471	1.151	0.28	0.78	3.64	1.28
36.11	4.253	1.471	1.151	0.27	0.78	3.70	1.28
42.49	4.303	1.471	1.151	0.27	0.78	3.74	1.28
48.66	4.327	1.471	1.151	0.27	0.78	3.76	1.28
60.00	4.327	1.471	1.151	0.27	0.78	3.76	1.28
80.00	4.327	1.471	1.151	0.27	0.78	3.76	1.28

*f, A are frequencies and amplifications for each site condition, with the value of V_{S30} (m/s) given by the subscript of A. The tabulated frequencies need to be closely spaced near 9 Hz to capture the resonant peak for A_{760}.

relative to the NSHM adjustment for $T = 0.1$ s. The agreement at $T = 0.1$ s of the NSHM adjustment with the $\kappa_0 = 0.03$ s adjustment of this study is coincidental.

The key conclusions to be drawn from Figure 6 are as follows: (1) there is little **M** or R_{RUP} dependence to the adjustment factors for $R_{RUP} < 100$ km and even at greater distances for longer periods, (2) the adjustment factors for short-period IMs are sensitive to κ_0 (this is also true for longer-period motions for very small events), and (3) there is good agreement between the FAS and PSA ratios for most magnitudes at $R_{RUP} < 100$ km and even at greater distances for longer periods. This last conclusion is important because it means that the simple FAS ratios given in Table 2 can be used in most cases for the IM adjustment factors over the range of parameters of greatest engineering interest, rather than needing to use the more involved tables in terms of **M** and R_{RUP} given in the Ⓔ electronic supplement.

The differences between the IM and the FAS adjustment factors are understandable in terms of the complex, combined effect of the frequency response of a single-degree-of-system oscillator, the magnitude- and frequency-dependent source spectral shape, the frequency-dependent amplification and diminution, and the distance- and magnitude-dependent path attenuation (see, for example, the discussion on p. 681 of Campbell and Boore, 2016). This is because there will always be a response of an oscillator to the input ground motion, even if there is little or no energy in the ground motion at the frequency of the oscillator, due to the broadband nature of PSA at periods shorter than the peak response, as demonstrated by many authors (e.g., Akkar *et al.*, 2011; Douglas and Boore, 2011; Bora *et al.*, 2016; Campbell and Boore, 2016).

Another way of displaying the adjustment factors is given in Figure 7, which shows the adjustment factors as

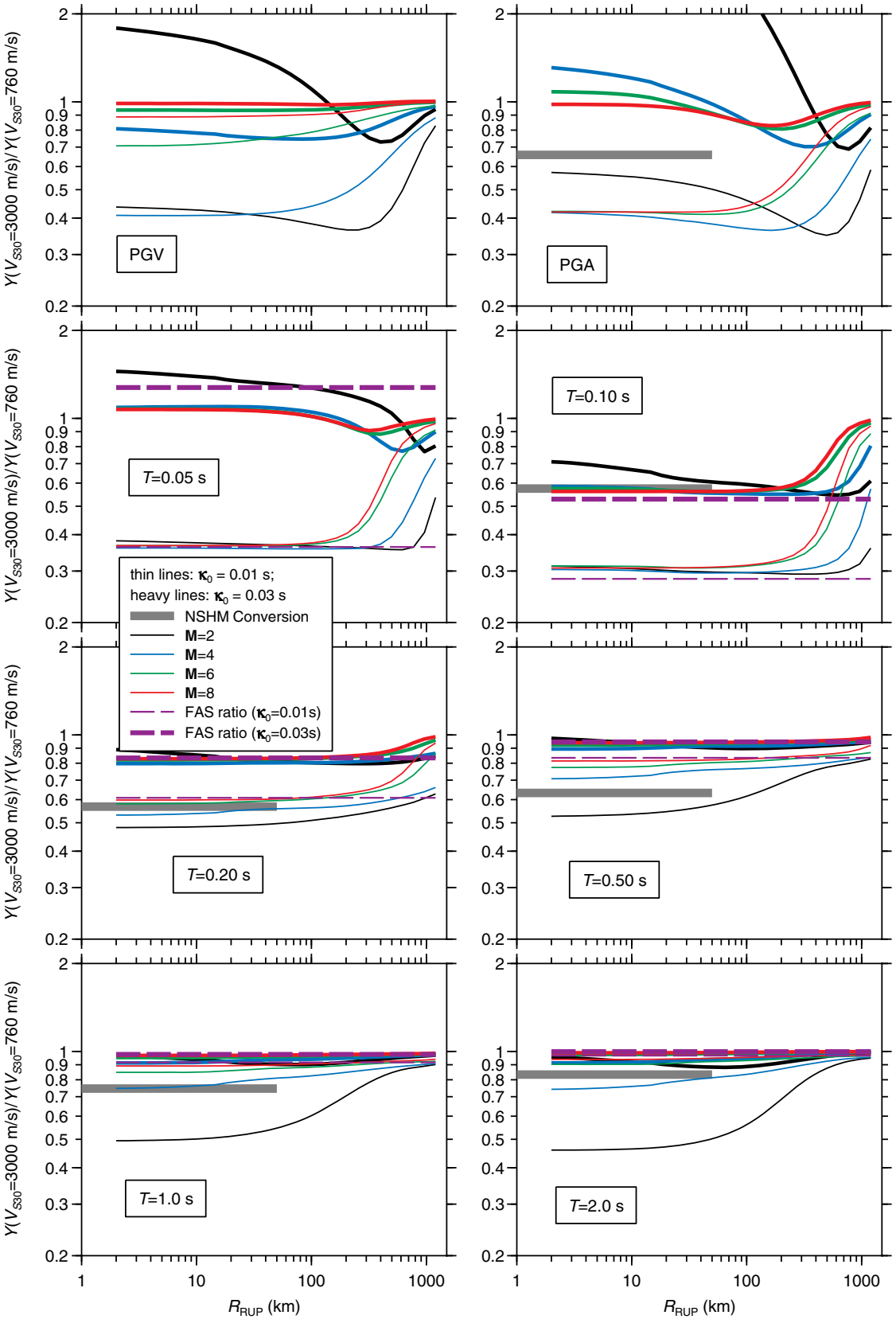

Figure 6. Ground-motion intensity measure (IM) adjustment factors for sites with V_{S30} = 760 and 3000 m/s as a function of rupture distance (R_{RUP}), for four values of moment magnitude (**M**) and two values of the diminution parameter κ_0. The adjustment factors for FAS, which are independent of **M** and R_{RUP}, but dependent on κ_0, are also shown. The color version of this figure is available only in the electronic edition.

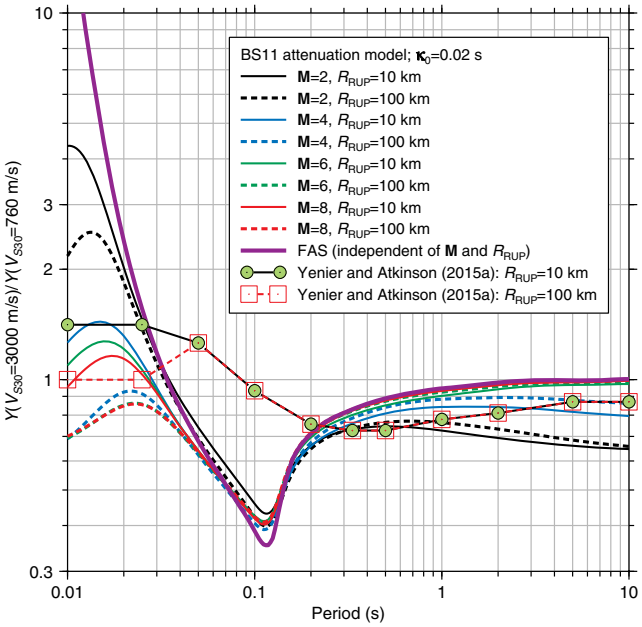

Figure 7. Ground-motion IM adjustment factors between sites with $V_{S30} = 3000$ and 760 m/s as a function of oscillator period for four values of moment magnitude (**M**), two values of rupture distance (R_{RUP}), and a single value of the diminution parameter ($\kappa_0 = 0.02$ s). The adjustment factors for FAS, which are independent of **M** and R_{RUP} but dependent on κ_0, are also shown as well as factors proposed by Yenier and Atkinson (2015a; see the Site Adjustment Factors for Ground-Motion Intensity Measures section). The color version of this figure is available only in the electronic edition.

a function of period for $\kappa_0 = 0.02$ s, four magnitudes, and two distances. Again, for comparison, the FAS adjustment factor is also shown. As stated before, FAS ratios are independent of **M** and R_{RUP} but are still dependent on κ_0 at high frequencies. The FAS ratios are close to the PSA ratios for periods near the peak of the B/C amplification factors for all **M**. The larger differences between FAS and PSA adjustment factors occur for small **M** at longer periods and for all **M** at shorter periods.

The adjustment factors from Yenier and Atkinson (2015a) are also included in Figure 7. Their adjustment factors are derived from the B/C and HR GMPEs in Atkinson and Boore (2006, 2007). Van Houtte *et al.* (2011) also gave HR to softer rock adjustment factors. They used the hybrid empirical method to adjust the HR GMPE developed by Campbell (2003, 2004) for CENA to a $V_{S30} = 800$ m/s reference-rock site condition appropriate for Europe using values of κ_0 that ranged from 0.02 to 0.05 s. Their adjustments (not shown here) differ from those in Figure 7 for $T < 0.2$ s in a manner consistent with the lack of a resonant peak in the assumed European crustal model (i.e., no dip at $T = 0.11$ s) and the use of higher values of κ_0 (i.e., a short-period peak that is shifted to a longer period). Because these previous studies based their adjustments on different assumptions about the HR and B/C amplifications than those used in this article, we do not expect perfect agreement with our adjustments. The major disagreement near 0.1 s is due to our inclusion of a resonant peak in our B/C amplifications (Fig. 4); the Atkinson and Boore (2006, 2007) B/C amplifications and the Van Houtte *et al.* (2011) $V_{S30} = 800$ m/s amplifications are based on a smooth V_S profile with no resonant peak. The comparison of the adjustments shown in Figure 7 is a good example of the importance of the resonance that we believe exists in CENA B/C sites, based on the profiles used in our study.

Values of κ_0 for CENA B/C Sites

The adjustment factors for short-period IMs are sensitive to the value of κ_0 (Fig. 6). The literature contains a wide range of proposed κ_0 values for CENA B/C sites (e.g., Campbell, 2009; Campbell *et al.*, 2014; PEER, 2015). For example, Fea96 proposed a value of $\kappa_0 = 0.01$ s, based on recordings obtained at the U.S. Department of Energy Savannah River Site. Darragh *et al.* (2015) found a κ_0 value of ~0.01 s (a value between 0.005 and 0.013 s for National Earthquake Hazards Reduction Program [NEHRP] site classes B and C) from a broadband inversion of CENA recordings. Silva *et al.* (1999), Atkinson and Boore (2006, 2007), Campbell (2007), Atkinson *et al.* (2014), and Hassani and Atkinson (2015) proposed a value of 0.02 s. Hollenback *et al.* (2015) and Yenier and Atkinson (2015b) used a value of 0.025 s. The $\kappa_0 = 0.01$ s value and corresponding V_S profile used by Fea96 to develop site factors to adjust IMs on HR to B/C site conditions was later shown by Campbell (2009) to be consistent with his proposed Q–V_S relationships and corresponding amplification factors. However, Campbell (2009) also showed that a $\kappa_0 = 0.02$ s value used in conjunction with the Fea96 V_S profile resulted in a short-period amplification factor that was more consistent with that in the 2009 edition of the NEHRP seismic provisions (Building Seismic Safety Council, 2009).

The database developed for the PEER NGA-East project has recordings at only nine stations for which there is a measured value of V_{S30} within a factor of 1.1 of 760 m/s, and most of those recordings are for earthquakes small enough that their corner frequencies might bias estimates of κ_0 obtained by the typical procedure of fitting a line to the logarithm of the FAS plotted against linear frequency (Anderson and Hough, 1984). Perhaps more importantly, most of the recordings are at great enough distances that whole-path attenuation will obscure the zero-distance diminution parameter κ_0. The only recordings at distances less than 50 km are from a single station in Oklahoma, which has a V_S profile less than 30 m in depth and does not show an indication of having a shallow depth to HR. For these reasons, there is little observational basis for determining κ_0 at CENA B/C sites. Instead, we turn to the ANZA seismic network Pinyon Flat Observatory (PFO) site in southern California, where the V_S profile is similar to B/C sites in CENA, and a large amount of ground-motion data are available from various types of instruments. Detailed information about the site geology and instrumentation

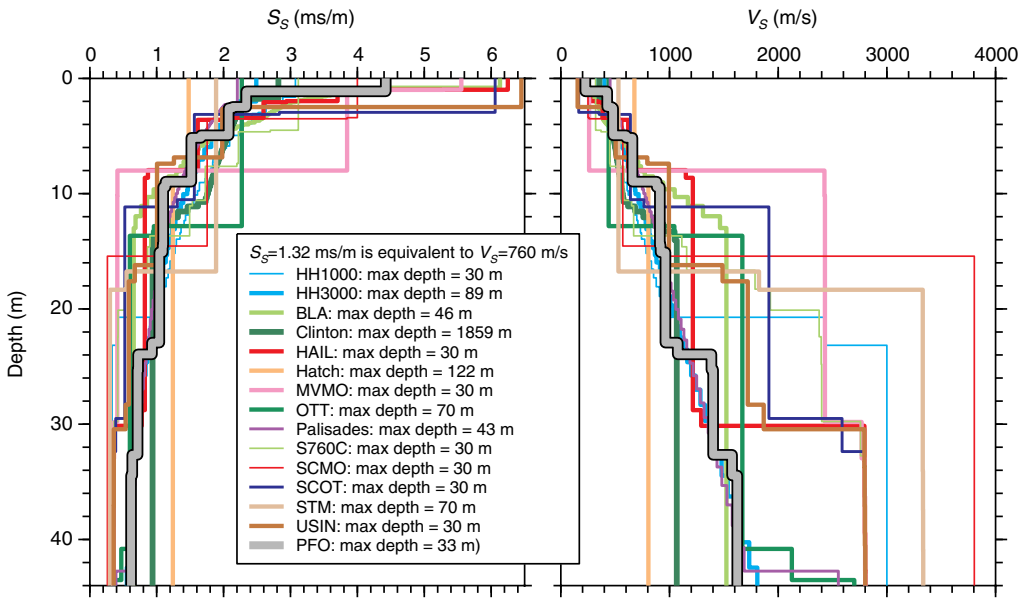

Figure 8. Shear-wave slowness and velocity versus depth at the California Pinyon Flat Observatory (PFO) site compared to the 14 central and eastern North America (CENA) sites used to derive the generic CENA B/C crustal amplification model. The color version of this figure is available only in the electronic edition.

of the PFO site are provided in Berger *et al.* (1984), Fletcher *et al.* (1990), and Aster and Shearer (1991a,b). According to Campbell *et al.* (2014), Silva *et al.* (1999) first proposed that the region near PFO might be analogous to the HR environment of CENA. Our PFO V_S profile is a composite made by combining the measured V_S profile of Yong *et al.* (2013), which has a maximum depth of 33 m, and the Southern California Earthquake Center (SCEC)-S4 Community Velocity Model (see Data and Resources). A comparison of this composite profile and the corresponding slowness profile with the 14 CENA profiles that we discussed previously is shown in Figure 8. It is clear that the slowness and velocity profiles at PFO are very similar to those at the CENA B/C sites. This similarity is the basis for concluding that κ_0 values obtained at PFO might be applicable to CENA B/C sites.

The diminution parameters κ (the value of κ at an arbitrary distance) and κ_0 at PFO has been estimated in a number of studies. Baltay and Hanks (2015) estimated κ_0 by simulating the magnitude dependence of PGA and PGV for small earthquakes (centered near **M** 2) recorded at PFO for earthquakes within 20 km of the site. Hough *et al.* (1988), Van Houtte *et al.* (2011), Kilb *et al.* (2012), and O.-J. Ktenidou (written comm., 2015) estimated κ from the FAS of recordings obtained at PFO. We repeated those estimates of both κ and κ_0 using different assumptions and different data and discuss the results briefly in the following section. Additional details can be obtained from the first author.

Estimates of κ_0 from Magnitude Scaling of PGA and PGV

Figure 9 shows values of PGA and PGV from recordings of 623 earthquakes within 20 km of PFO as a function of magnitude. The data are from the PFO broadband station of the ANZA seismic network situated close to the location from which the measurements used to obtain the slowness and V_S profiles shown in Figure 8 were made. The data were provided by A. Baltay (written comm., 2016). The depth distribution of earthquakes close to PFO is somewhat bimodal, with concentrations near 8 and 13 km. To avoid possible scatter using sets of data from two concentrations of depths, we only show data in Figure 9 for which the earthquake depth is greater than 10 km. The same conclusions are reached if the shallower data are used. The PGA and PGV values are geometric means of the peak values from the two horizontal components from each recording. The peak values were adjusted to a hypocentral distance of 10 km using a modification of the Boore *et al.* (2014) GMPE distance-dependence term that uses the event's hypocentral depth rather than a generic pseudodepth term, and does not allow an **M** dependence of the geometrical spreading term. The simulations were done using the time-domain module *tmrsk_loop_td_drvr* (see Data and Resources) in the stochastic simulation program SMSIM (Boore, 2005), together with a single-corner-frequency source spectrum, the Raoof *et al.* (1999) geometrical spreading and Q terms, the Boore and Thompson (2014) path durations, and crustal amplifications computed for the PFO composite slowness model using the SRI method of Boore (2013). The parameter file for the runs is given in the Ⓔ electronic supplement. As shown in Figure 9, the simulations were done for a suite of κ_0 values ranging from 0.006 to 0.080 s. The value of 0.006 s (Campbell *et al.*, 2014), together with a V_{S30} value of 3000 m/s (Hashash, Kottke, Stewart, Campbell, Kim, Moss, *et al.*, 2014; Hashash, Kottke, Stewart, Campbell, Kim, Rathje, and Silva 2014), was used to define reference-rock site condi-

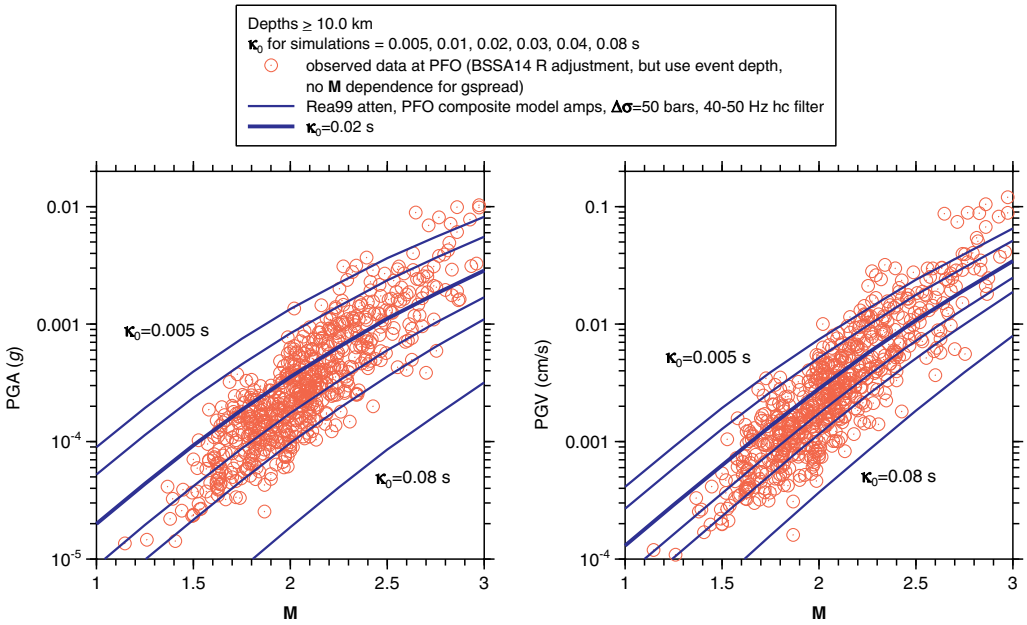

Figure 9. Observed and simulated magnitude scaling of peak ground acceleration (PGA) and peak ground velocity (PGV) recorded at PFO. The data shown in these graphs were provided by A. Baltay (written comm., 2016) and were corrected to a horizontal distance of 10 km using a modified version of the attenuation term in Boore *et al.* (2014). The simulations used the Raoof *et al.* (1999; hereafter, Rea99) geometric and anelastic attenuation model and crustal amplifications based on the PFO composite velocity model, which combined the preferred model of Yong *et al.* (2013) for depths less than 33 m with the Southern California Earthquake Center (SCEC)-S4 Community Velocity Model for the location of PFO at greater depths. The color version of this figure is available only in the electronic edition.

tions in the NGA-East project. Although the scatter is large, the mass of data near **M** 2 is consistent with simulations using a value of κ_0 near 0.02 s, shown by the heavy lines in Figure 9. This is true for both PGA and PGV. We acknowledge that the observed **M**-scaling slope is not perfectly captured by the simulations. We tried many simulations to match better the magnitude-dependent slope in the data, including varying the average radiation pattern, stress parameter, value of the high-cut filter (near 50 Hz), crustal amplification (e.g., no amplification and full-resonant amplification), and path duration, without success. We found that either the parameters required to fit the trend were unrealistic (e.g., a path duration exceeding 30 s for small events) or improving the data–simulation comparison for PGA led to a worse comparison for PGV and vice versa. Using a similar method, but with a different subset of the data and different model assumptions, Baltay and Hanks (2015) found the values of κ_0 shown in Figure 10.

Estimates of κ_0 from Fourier Displacement and Acceleration Spectra

Building on the pioneering work of Anderson and Hough (1984), a number of authors have determined κ from the FAS of data recorded at PFO. The usual spectral-decay method involves fitting a straight line to the high-frequency part of a plot of the logarithm of FAS plotted against linear frequency, as originally proposed by Anderson and Hough (1984). For very small earthquakes, for which the corner frequency is so high it masks the effect of κ on the attenuation of the FAS at high frequencies, an alternative method is to fit a straight line to the low-frequency part of the logarithm of the Fourier displacement spectrum plotted against linear frequency (e.g., Ktenidou *et al.*, 2014). The resulting estimates of κ from several authors are shown in Figure 10. Included in this figure are estimates from a number of recordings that were not used in previously published estimates; the events used by us are given in Table 3.

Before discussing the results, it is important to point out that the recordings from which κ estimates were made come from two sites at Pinyon Flat, separated by 675 m. The sources of the data are indicated in the legend of Figure 10 by the prefixes PFO and USGS 5044. The values from Van Houtte *et al.* (2011), O.-J. Ktenidou (personal comm., 2015), and the events in Table 3 are from recordings at USGS station 5044; those of Hough *et al.* (1988), Kilb *et al.* (2012), and two events with magnitudes of 5.0 and 5.2, whose κ values were determined by the first author, are from the ANZA seismic network station PFO (the instrumentation and station abbreviation may have changed over time, but the spatial locations are similar and are more than 600 m distant from USGS station 5044). The slowness and V_S profiles shown in Figure 8 are based on measurements near PFO and not near USGS station 5044. Although the topography is relatively flat, and large lateral changes in the V_S are not expected, there are some suggestions that lateral changes do occur (A. Yong, personal comm., 2015).

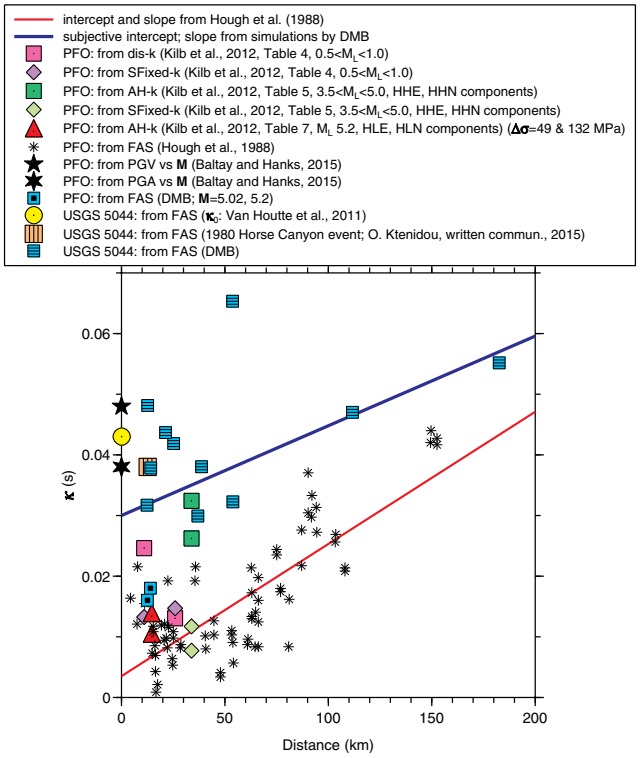

Figure 10. A composite of κ determinations at California Pinyon Flat sites PFO and U.S. Geological Survey (USGS) 5044 by various authors, including the first author (DMB), obtained from FAS using the spectral-decay method. The color version of this figure is available only in the electronic edition.

The first estimates of κ at Pinyon Flat were those from recordings at PFO by Hough *et al.* (1988; see Fig. 10). Assuming a linear dependence of κ on distance, these authors extrapolated their estimates to zero distance to infer $\kappa_0 = 0.0035$ s. There are several reasons why this value might be too low. First, as acknowledged by Hough *et al.* (1988), there is no reason to expect that a linear dependence is expected, although they say that it is a reasonable first-order approximation. Later, Anderson (1991) used a non-parametric distance term to characterize the decrease in κ with distance using these same recordings. Assuming a common distance shape for the function at all stations in the ANZA seismic network, a joint inversion of the data from all stations resulted in a flattening of κ with distance between about 20 and 60 km (this flattening can be seen in the Hough *et al.*, 1988, values shown in our Fig. 10). Extrapolating this portion of the function fit to the PFO κ observations of Hough *et al.* (1988) results in κ_0 estimates of about 0.012 s (Anderson, 1991, reports $\kappa_0 = 0.0036$ s, but as shown in his fig. 1, that conclusion assumes a downturn in the attenuation for distances less than 20 km that is not consistent with the data at PFO). The second reason is that the corner frequencies of a number of events used by Hough *et al.* (1988), for which the magnitudes ranged from about 1.7 to 4.4, with many events having magnitudes less than 3.0 (as shown in Fig. 2 of Hough *et al.*, 1988), might be high enough to interact with the effect of κ on the shape of the FAS, leading to a biased estimate of κ_0. To assess the importance of this potential bias, we did a simulation study in which synthetic acceleration time series were generated for a wide range of magnitudes and distances and for κ_0 values of 0.01, 0.02, and 0.04 s. The FAS for these simulated acceleration time series were computed, from which the values of κ were estimated using the same methods as for the recorded data. We then fit lines to the κ versus distance plots and extrapolated these back to zero distance to estimate κ_0. A definite bias was found, with the value of κ_0 from the simulated FAS being lower than the value of κ_0 used in the simulations, with the bias being larger for smaller earthquakes. By considering the magnitudes used by Hough *et al.* (1988), we concluded from the simulation study that the Hough *et al.* (1988) values of κ are too low by about 0.01 s on average. Correcting for this bias implies that the values of κ at PFO estimated by Hough *et al.* (1988) are consistent with $\kappa_0 \approx 0.015$ s. This latter value is also more consistent with the $\kappa_0 = 0.01$ s value calculated by Silva and Darragh (1995) from fitting response spectra computed from recordings, and it is consistent with a number of the values reported by Kilb *et al.* (2012) and the

Table 3
Events Recorded at Pinyon Flat U.S. Geological Survey Station 5044 for Which κ Was Determined in This Article from Fitting the Spectral Decay of FAS

Event Name	Year	Month/Date	Hr:Min	Magnitude	Type	R_{epi} (km)	Depth (km)	R_{hyp} (km)
Anza (Horse Canyon)	1980			5.2	**M**	12.7	13.6	18.6
Hector Mine	1999			7.1	**M**	111.7	14.8	112.6
Anza-02	2001			4.9	**M**	12.4	15.2	19.6
Borrego Springs	2002			4.2	M_L	25.2	2.7	25.4
Desert Hot Springs	2005			4.1	**M**	38.7	7.5	39.4
Anza	2005			5.2	**M**	14.2	14.1	20.0
Mt. San Gorgonio	2005	10/18	4:08	3.9	**M**	53.9	15.9	56.2
Mt. San Gorgonio	2005	10/18	7:31	4.2	**M**	53.7	17.0	56.4
Thousand Palms	2007			4.4	**M**	36.9	4.8	37.2
Sierra El Major	2010	04/04		7.2	**M**	196.3	10.0	196.6
Collins Valley	2010			5.4	**M**	21.3	11.7	24.3

R_{epi}, epicentral distance; R_{hyp}, hypocentral distance.

first author (labeled DMB) from data at the PFO station, as shown in Figure 10.

As shown in Figure 10, κ estimates from data recorded at USGS station 5044 are consistently larger than those from data at PFO by about 0.01–0.02 s. Overall, considering both the fit to PGA and PGV versus magnitude and the values of κ_0 implied by fitting FAS to stochastic simulations described previously, it seems that $\kappa_0 = 0.01$–0.03 s is a reasonable range for the PFO B/C site. This range is also consistent with the values of κ_0 that have been proposed for CENA B/C sites for use in stochastic simulations, as discussed previously. This range is the basis for the κ_0 values used in the adjustment factors shown in Figures 6 and 7.

Summary

Many times it is necessary to adjust ground motions between sites. For example, adjustments are needed in constructing seismic-hazard maps for a B/C site condition when many of the GMPEs used in deriving the maps are for harder rock conditions (Frankel *et al.*, 1996, 2002; Petersen *et al.*, 2008, 2014). Another example is in comparisons of motions from NGA-East ground-motion models, for which the site condition is specified by $V_{S30} = 3000$ m/s, with recorded ground motions, for which most of the motions come from sites with estimated values of V_{S30} near 500 m/s. There are no records in the NGA-East database at very hard sites, however, so we cannot determine adjustment factors empirically. A procedure to adjust motions between various reference-rock site conditions is given in this study. The first step is to adjust the observed motions to a $V_{S30} = 760$ m/s firm-rock (NEHRP B/C) site condition, then use adjustment factors to convert that motion to a site with $V_{S30} = 3000$ m/s. Our results are for a B/C site characterized by a velocity increase to much higher velocities at relatively shallow depths. Examples of such sites might be those with a layer of till over glaciated bedrock or low-velocity sediments overlying Paleozoic carbonate rocks, such that the time-averaged velocity to 30 m is 760 m/s. There could be other types of sites in CENA for which V_{S30} is 760 m/s, but we have no observational basis to propose adjustment factors for such sites, although some guidance is given in Campbell (2009). The adjustment of motions from soil- and soft-rock sites to sites with $V_{S30} = 760$ m/s was not addressed in our study, because it is the subject of simulated and empirical site-response studies being conducted by the NGA-East Geotechnical Working Group (e.g., Harmon, 2016; Harmon *et al.*, 2016; Parker *et al.*, 2016). Our study focuses on the adjustments from $V_{S30} = 760$ m/s to $V_{S30} = 3000$ m/s and vice versa, but we also provide adjustments for sites with $V_{S30} = 2000$ m/s to those with $V_{S30} = 3000$ m/s, because a number of the recordings in northeastern United States and southeastern Canada are from sites for which the estimated V_{S30} is near 2000 m/s. The adjustment factors are based on stochastic-method simulations (Boore, 2003), using the FAS crustal amplifications described in this article. Adjustment factors are provided as tables of ratios of simulated IMs for sites with $V_{S30} = 3000$ m/s and sites with either $V_{S30} = 760$ or 2000 m/s. The adjustment factors are for magnitudes (**M**) ranging from 2 to 8, for rupture distances (R_{RUP}) ranging from 2 to 1200 km, and for PSA for spectral periods (T) ranging from 0.01 to 10 s, PGA, and PGV. One V_S profile was considered for the $V_{S30} = 3000$ m/s site, because the amplifications are not sensitive to the details of HR slowness profiles. In contrast, we used 14 CENA slowness profiles with V_{S30} values within a factor of 1.1 of 760 m/s, because variations in these profiles were found to have a significant impact on the mean adjustment factors. The adjustment factors are provided for κ_0 values of 0.006, 0.01, 0.02, and 0.03 s, because of the large degree of epistemic uncertainty associated with the parameter.

The $V_{S30} = 760$ m/s amplifications in this article are for a generic site; we caution against combining these amplifications with amplifications for site-specific velocity profiles. Such amplifications should be computed using site-specific velocity profiles that extend to depths below any significant impedance contrasts, as we have done for the individual sites whose amplifications are shown in Figure 3.

The adjustment factors for each model are sensitive to the value of κ_0 at short periods. For a given value of T or f, the adjustment factors can be a function of magnitude and distance, but we note that, except for short-period motions ($T < \approx 0.04$ s), small magnitudes ($\mathbf{M} < \approx 3$), and large distances ($R_{\mathrm{RUP}} > 200$ km), the actual factors are relatively insensitive to **M** and R_{RUP}. For these cases, the ratios of the FAS of the ground motions (which are essentially ratios of the site amplifications) are a convenient substitute for the more complicated adjustment factors based on the ratios of simulated IMs. The FAS amplification factors and associated adjustment factors for $\kappa_0 = 0$ s are given in Table 2. These factors are not a function of magnitude and distance. Similar tables for PSA, PGA, and PGV, which are a function of magnitude and distance (except as noted previously), are presented in the Ⓔ electronic supplement.

Analysis of data from Pinyon Flat, California, for which the shear-wave slowness profile is very similar to that expected at a CENA site with V_{S30} close to 760 m/s (a site falling at the NEHRP B/C boundary), suggests that the value of κ_0 at such a site ranges from about 0.01 to 0.03 s, in the range of values proposed by several authors for use with B/C sites in CENA.

Data and Resources

The velocities used to create Figure 1 were taken from the Pacific Earthquake Engineering Research (PEER) Next Generation Attenuation-East (NGA-East) flatfile *NGA-East_RotD50_5pct_Flatfile_Public_20141118.xlsx*, as contained in NGA East Database eAppendices.zip link under the entry for PEER 2014/17—PEER NGA-East Database, available from http://peer.berkeley.edu/publications/peer_reports/reports_2014/reports_2014.html (last accessed October 2016). The

square-root-impedance (SRI) and full resonant amplifications shown in Figures 3 and 4 were computed using the programs *site_amp_batch* and *nrattle*, respectively; they and various utility programs used in the computations are part of the Stochastic-Method SIMulation (SMSIM) suite of programs (Boore, 2005), available from the online software link at www.daveboore.com (last accessed October 2016). The program *nrattle* is a modification by R. Herrmann of C. Mueller's program *rattle*; *nrattle* is included in the SMSIM suite of software with their permission. The densities used in some of the models were obtained from velocity–density relations given in Boore (2016). The ground-motion intensity measures (IMs) and the Fourier amplitude spectra (FAS) shown in Figures 5–7 were computed using the SMSIM programs *tmrsk_loop_rv_drvr* and *fmrsk_loop_fas_drvr*, respectively, whereas the simulations shown in Figure 9 were computed using the SMSIM program *tmrsk_loop_td_drvr*. The figures were prepared using CoPlot (http://www.cohort.com, last accessed October 2016).

Acknowledgments

We thank Joseph Harmon, Youssef Hashash, Walt Silva, Rob Williams, and Alan Yong for providing velocity models; Christine Goulet for encouragement and numerous conversations; Rob Graves for providing the Southern California Earthquake Center (SCEC)-S4 Community Velocity Model velocity profile at Pinyon Flat; Annemarie Baltay for providing peak ground acceleration (PGA) and peak ground velocity (PGV) data from Pinyon Flat Observatory (PFO) and many enlightening conversations; Chris Stephens for data from U.S. Geological Survey (USGS) station 5044 at Pinyon Flat; Olga Ktenidou for providing her estimates of κ at PFO; and Annemarie Baltay, Carola Di Alessandro, Suzanne Hecker, Keith Knudsen, Jon Stewart, and an anonymous reviewer for their constructive reviews.

References

Akkar, S., Ö. Kale, E. Yenier, and J. J. Bommer (2011). The high-frequency limit of usable response spectral ordinates from filtered analogue and digital strong-motion accelerograms, *Earthq. Eng. Struct. Dynam.* **40,** 1387–1401.

Anderson, J. G. (1991). A preliminary descriptive model for the distance dependence of the spectral decay parameter in southern California, *Bull. Seismol. Soc. Am.* **81,** 2186–2193.

Anderson, J. G., and S. E. Hough (1984). A model for the shape of the Fourier amplitude spectrum of acceleration at high frequencies, *Bull. Seismol. Soc. Am.* **74,** 1969–1993.

Aster, R. C., and P. M. Shearer (1991a). High-frequency borehole seismograms recorded in the San Jacinto fault zone, southern California. Part 1. Polarizations, *Bull. Seismol. Soc. Am.* **81,** 1057–1080.

Aster, R. C., and P. M. Shearer (1991b). High-frequency borehole seismograms recorded in the San Jacinto fault zone, southern California. Part 2. Attenuation and site effects, *Bull. Seismol. Soc. Am.* **81,** 1081–1100.

Atkinson, G. M., and D. M. Boore (2006). Earthquake ground-motion prediction equations for eastern North America, *Bull. Seismol. Soc. Am.* **96,** 2181–2205.

Atkinson, G. M., and D. M. Boore (2007). Erratum to "Earthquake ground-motion prediction equations for eastern North America", *Bull. Seismol. Soc. Am.* **97,** 1032.

Atkinson, G. M., D. W. Greig, and E. Yenier (2014). Estimation of moment magnitude (M) for small events (M <4) on local networks, *Seismol. Res. Lett.* **85,** 1116–1124.

Baltay, A. S., and T. C. Hanks (2015). Using PGA and PGV data to easily estimate station specific kappa, Abstract, *Seismol. Res. Lett.* **86,** 662.

Beresnev, I. A., and G. M. Atkinson (1997). Shear-wave velocity survey of seismographic sites in eastern Canada: Calibration of empirical regression method of estimating site response, *Seismol. Res. Lett.* **68,** 981–987.

Berger, J., L. M. Baker, J. N. Brune, J. B. Fletcher, T. C. Hanks, and F. L. Vernon III (1984). The Anza array: A high-dynamic-range, broadband, digitally radiotelemetered, seismic array, *Bull. Seismol. Soc. Am.* **74,** 1469–1481.

Boatwright, J., and L. Seekins (2011). Regional spectral analysis of three moderate earthquakes in northeastern North America, *Bull. Seismol. Soc. Am.* **101,** 1769–1782.

Boore, D. M. (2003). Simulation of ground motion using the stochastic method, *Pure Appl. Geophys.* **160,** 635–676.

Boore, D. M. (2005). SMSIM—Fortran programs for simulating ground motions from earthquakes: Version 2.3, a revision of OFR 96-80-A, Revised 15 August 2005, *U.S. Geol. Surv. Open-File Rept. 00-509*, 55 pp.

Boore, D. M. (2012). Updated determination of stress parameters for nine well-recorded earthquakes in eastern North America, *Seismol. Res. Lett.* **83,** 190–199.

Boore, D. M. (2013). The uses and limitations of the square-root impedance method for computing site amplification, *Bull. Seismol. Soc. Am.* **103,** 2356–2368.

Boore, D. M. (2015a). Adjusting ground-motion intensity measures to a reference site for which $V_{S30} = 3000$ m/s, *PEER Report 2015/06*, Pacific Earthquake Engineering Research Center, University of California, Berkeley, California, 85 pp.

Boore, D. M. (2015b). Point-source stochastic-method simulations of ground motions for the PEER NGA-East Project, chapter 2, in *NGA-East: Median Ground-Motion Models for the Central and Eastern North America Region, PEER Report 2015/04*, Pacific Earthquake Engineering Research Center, University of California, Berkeley, California, 11–49.

Boore, D. M. (2016). Determining generic velocity and density models for crustal amplification calculations, with an update of the Boore and Joyner (1997) generic site amplification for $\bar{V}_S(Z) = 760$ m/s, *Bull. Seismol. Soc. Am.* **106,** 316–320.

Boore, D. M., and W. B. Joyner (1997). Site amplifications for generic rock sites, *Bull. Seismol. Soc. Am.* **87,** 327–341.

Boore, D. M., and E. M. Thompson (2007). On using surface-source downhole-receiver logging to determine seismic slownesses, *Soil Dynam. Earthq. Eng.* **27,** 971–985.

Boore, D. M., and E. M. Thompson (2014). Path durations for use in the stochastic-method simulation of ground motions, *Bull. Seismol. Soc. Am.* **104,** 2541–2552.

Boore, D. M., and E. M. Thompson (2015). Revisions to some parameters used in stochastic-method simulations of ground motion, *Bull. Seismol. Soc. Am.* **105,** 1029–1041.

Boore, D. M., K. W. Campbell, and G. M. Atkinson (2010). Determination of stress parameters for eight well-recorded earthquakes in eastern North America, *Bull. Seismol. Soc. Am.* **100,** 1632–1645.

Boore, D. M., J. P. Stewart, E. Seyhan, and G. M. Atkinson (2014). NGA-West2 equations for predicting PGA, PGV, and 5%-damped PSA for shallow crustal earthquakes, *Earthq. Spectra* **30,** 1057–1085.

Bora, S. S., F. Scherbaum, N. Kuehn, and P. Stafford (2014). Fourier spectral- and duration models for the generation of response spectra adjustable to different source-, propagation-, and site conditions, *Bull. Earthq. Eng.* **12,** 467–493.

Bora, S. S., F. Scherbaum, N. Kuehn, and P. Stafford (2016). On the relationship between Fourier and response spectra: Implications for the adjustment of empirical ground-motion prediction equations (GMPEs), *Bull. Seismol. Soc. Am.* **106,** 1235–1253.

Bora, S. S., F. Scherbaum, N. Kuehn, P. Stafford, and B. Edwards (2015). Development of a response spectral ground-motion prediction equation (GMPE) for seismic-hazard analysis from empirical Fourier spectral and duration models, *Bull. Seismol. Soc. Am.* **105,** 2192–2218.

Brown, L. T., D. M. Boore, and K. H. Stokoe (2002). Comparison of shear-wave slowness profiles at ten strong-motion sites from non-invasive SASW measurements and measurements made in boreholes, *Bull. Seismol. Soc. Am.* **92,** 3116–3133.

Building Seismic Safety Council (2004). NEHRP Recommended Provisions for Seismic Regulations for New Buildings and other Structures (FEMA 450), Part 1: Provisions, Part 2: Commentary, 2003 Edition, National Institute of Building Sciences, Washington, D.C., available at http://www.nibs.org/?page=bssc_2003pubs#FEMA450 (last accessed November 2016).

Building Seismic Safety Council (2009). NEHRP Recommended Seismic Provisions for New Buildings and other Structures (FEMA P-750), 2009 Edition, National Institute of Building Sciences, Washington, D.C.

Campbell, K. W. (2003). Prediction of strong ground motion using the hybrid empirical method and its use in the development of ground-motion (attenuation) relations in eastern North America, *Bull. Seismol. Soc. Am.* **93,** 1012–1033.

Campbell, K. W. (2004). Erratum to "Prediction of strong ground motion using the hybrid empirical method and its use in the development of ground-motion (attenuation) relations in eastern North America", *Bull. Seismol. Soc. Am.* **94,** 418.

Campbell, K. W. (2007). Validation and update of hybrid empirical ground motion (attenuation) relations for the CEUS, NEHRP External Research Program, *U.S. Geol. Surv. Final Technical Rept.*, Award No. 05HQGR0032.

Campbell, K. W. (2009). Estimates of shear-wave Q and κ_0 for unconsolidated and semiconsolidated sediments in eastern North America, *Bull. Seismol. Soc. Am.* **99,** 2365–2392.

Campbell, K. W., and D. M. Boore (2016). Evaluation of six NEHRP B/C crustal amplification models proposed for use in western North America, *Bull. Seismol. Soc. Am.* **106,** 673–686.

Campbell, K. W., Y. M. A. Hashash, B. Kim, A. R. Kottke, E. M. Rathje, W. J. Silva, and J. P. Stewart (2014). Reference-rock site conditions for central and eastern North America: Part II—Attenuation definition, *PEER Report 2014-12*, Pacific Earthquake Engineering Research Center, University of California, Berkeley, California, 80 pp.

Darragh, R. B., N. A. Abrahamson, W. J. Silva, and N. Gregor (2015). Development of hard rock ground motion models for region 2 of central and eastern North America, chapter 3, in *NGA-East: Median Ground Motion Models for the Central and Eastern North America Region, PEER Report 2015/04*, Pacific Earthquake Engineering Research Center, University of California, Berkeley, California, 51–84.

Douglas, J., and D. M. Boore (2011). High-frequency filtering of strong-motion records, *Bull. Earthq. Eng.* **9,** 395–409.

Dreiling, J., M. P. Isken, W. D. Mooney, M. C. Chapman, and R. W. Godbee (2014). NGA-East regionalization report: Comparison of four crustal regions within central and eastern North America using waveform modeling and 5%-damped pseudo-spectral acceleration response, *PEER Report 2014/15*, Pacific Earthquake Engineering Research Center, University of California, Berkeley, California, 218 pp.

Fletcher, J. B., T. Fumal, H.-P. Liu, and L. C. Carroll (1990). Near-surface velocities and attenuation at two boreholes near Anza, California, from logging data, *Bull. Seismol. Soc. Am.* **80,** 807–831.

Frankel, A., C. Mueller, T. Barnhard, D. Perkins, E. Leyendecker, N. Dickman, S. Hanson, and M. Hopper (1996). National seismic hazard maps: Documentation June 1996, *U.S. Geol. Surv. Open-File Rept. 96-532*, 69 pp.

Frankel, A. D., M. D. Petersen, C. S. Mueller, K. M. Haller, R. L. Wheeler, E. V. Leyendecker, R. L. Wesson, S. C. Harmsen, C. H. Cramer, D. M. Perkins, *et al.* (2002). Documentation for the 2002 update of the national seismic hazard maps, *U.S. Geol. Surv. Open-File Rept. 02-420*, 39 pp.

Goulet, C. A., T. Kishida, T. D. Ancheta, C. H. Cramer, R. B. Darragh, W. J. Silva, Y. M. A. Hashash, J. Harmon, J. P. Stewart, K. E. Wooddell, *et al.* (2014). PEER NGA-East Database, *PEER Report 2014/17*, Pacific Earthquake Engineering Research Center, University of California, Berkeley, California, 97 pp.

Harmon, J. A. (2016). Nonlinear site amplification functions for central and eastern North America, *Dissertation*, Department of Civil and Environmental Engineering, University of Illinois at Urbana–Champaign, Champaign, Illinois.

Harmon, J. A., Y. M. A. Hashash, J. P. Stewart, E. M. Rathje, K. W. Campbell, W. J. Silva, and G. Parker (2016). A simulation-based ground response model to guide development of a generalized site amplification model for central and eastern North America, Abstract, *Seismol. Res. Lett.* **87,** 554.

Hashash, Y. M. A., A. R. Kottke, J. P. Stewart, K. W. Campbell, B. Kim, C. Moss, S. Nikolaou, E. M. Rathje, and W. J. Silva (2014). Reference rock site condition for central and eastern North America, *Bull. Seismol. Soc. Am.* **104,** 684–701.

Hashash, Y. M. A., A. R. Kottke, J. P. Stewart, K. W. Campbell, B. Kim, E. M. Rathje, and W. J. Silva (2014). Reference-rock site conditions for central and eastern North America: Part I—Velocity definition, *PEER Report 2014/11*, Pacific Earthquake Engineering Research Center, University of California, Berkeley, California, 188 pp.

Hassani, B., and G. M. Atkinson (2015). Referenced empirical ground-motion model for eastern North America, chapter 10, in *NGA-East: Median Ground-Motion Models for the Central and Eastern North America Region, PEER Report 2015/04*, University of California, Berkeley, California, 251–272.

Hollenback, J., N. Kuehn, C. Goulet, and N. A. Abrahamson (2015). PEER NGA-East median ground motion models, chapter 11, in *NGA-East: Median Ground Motion Models for the Central and Eastern North America Region, PEER Report 2015/04*, Pacific Earthquake Engineering Research Center, University of California, Berkeley, California, 273–309.

Hough, S. E., J. G. Anderson, J. Brune, J. Vernon III, F. Berger, J. Fletcher, L. Haar, T. Hanks, and L. Baker (1988). Attenuation near Anza, California, *Bull. Seismol. Soc. Am.* **78,** 672–691.

Kilb, D., G. Biasi, J. Anderson, J. Brune, Z. Peng, and F. L. Vernon (2012). A comparison of spectral parameter kappa from small and moderate earthquakes using southern California ANZA Seismic Network data, *Bull. Seismol. Soc. Am.* **102,** 284–300.

Ktenidou, O.-J., F. Cotton, N. A. Abrahamson, and J. G. Anderson (2014). Taxonomy of kappa: A review of definitions and estimation approaches targeted to applications, *Seismol. Res. Lett.* **85,** 135–146.

Odum, J. K., W. J. Stephenson, and R. A. Williams (2010). Predicted and observed spectral response from collocated shallow, active and passive-source V_S data at five ANSS sites, Illinois and Indiana, USA, *Seismol. Res. Lett.* **81,** 955–964.

Pacific Earthquake Engineering Research Center (PEER) (2015). NGA-East: Median ground-motion models for central and eastern North America, *PEER Report 2015/04*, University of California, Berkeley, California, 322 pp.

Parker, G. A., J. P. Stewart, Y. M. A. Hashash, E. M. Rathje, K. W. Campbell, W. J. Silva, and J. Harmon (2016). Empirical seismic site amplification in central and eastern North America from NGA-East ground motion database, Abstract, *Seismol. Res. Lett.* **87,** 555.

Petersen, M. D., A. D. Frankel, S. C. Harmsen, C. S. Mueller, K. M. Haller, R. L. Wheeler, R. L. Wesson, Y. Zeng, O. S. Boyd, D. M. Perkins, *et al.* (2008). Documentation for the 2008 update of the United States national seismic hazard maps, *U.S. Geol. Surv. Open-File Rept. 2008–1128*, 128 pp.

Petersen, M. D., M. P. Moschetti, P. M. Powers, C. S. Mueller, K. M. Haller, A. D. Frankel, Y. Zeng, S. Rezaeian, S. C. Harmsen, O. S. Boyd, *et al.* (2014). Documentation for the 2014 update of the United States national seismic hazard maps, *U.S. Geol. Surv. Open-File Rept. 2014–1091*, 243 pp.

Pezeshk, S., A. Zandieh, K. W. Campbell, and B. Tavakoli (2015). Ground-motion prediction equations for CENA using the hybrid empirical method in conjunction with NGA-West2 empirical ground-motion models, chapter 5, in *NGA-East: Median Ground-Motion Models for the Central and Eastern North America Region, PEER Report 2015/04*, Pacific Earthquake Engineering Research Center, University of California, Berkeley, California, 117–147.

Raoof, M., R. B. Herrmann, and L. Malagnini (1999). Attenuation and excitation of three-component ground motion in southern California, *Bull. Seismol. Soc. Am.* **89,** 888–902.

Read, K., H. El Naggar, and D. Eaton (2008). Site-response spectra for Polaris station sites in southern Ontario and Quebec, *Seismol. Res. Lett.* **79,** 776–784.

Rovey, C. W., II, and G. Balco (2011). Summary of early and middle Pleistocene glaciations in northern Missouri, USA, in *Developments in Quaternary Science*, J. Ehlers, P. L. Gibbard, and P. D. Hughes (Editors), Vol. 15, Chap. 43, Elsevier, Amsterdam, The Netherlands, 553–561.

Seyhan, E., and J. P. Stewart (2014). Semi-empirical nonlinear site amplification from NGA-West 2 data and simulations, *Earthq. Spectra* **30,** 1241–1256.

Shahjouei, A., and S. Pezeshk (2015). Hybrid empirical ground-motion model for central and eastern North America using hybrid broadband simulations and NGA-West2 GMPES, chapter 7, in *NGA-East: Median Ground- Motion Models for the Central and Eastern North America Region, PEER Report 2015/04*, University of California, Berkeley, California, 165–192.

Silva, W. J., and R. B. Darragh (1995). Engineering characterization of earthquake strong ground motion recorded at rock sites, *EPRI TR-102262*, Electric Power Research Institute, Palo Alto, California.

Silva, W. J., R. B. Darragh, N. N. Gregor, G. Martin, N. A. Abrahamson, and C. Kircher (1999). Reassessment of site coefficients and near-fault factors for building code provisions, NEHRP External Research Program, *U.S. Geol. Surv. Final Technical Rept.*, Award Number 98HQGR1010.

Van Houtte, C., S. Drouet, and F. Cotton (2011). Analysis of the origins of κ (kappa) to compute hard rock to rock adjustment factors for GMPEs, *Bull. Seismol. Soc. Am.* **101,** 2926–2941.

Williams, R. A., J. K. Odum, W. J. Stephenson, and R. B. Herrmann (2007). Shallow *P*- and *S*-wave velocities and site resonances in the St. Louis region, Missouri-Illinois, *Earthq. Spectra* **23,** 711–726.

Yenier, E., and G. M. Atkinson (2015a). Regionally-adjustable generic ground-motion prediction equation based on equivalent point-source simulations: Application to central and eastern North America, chapter 4, in *NGA-East: Median Ground- Motion Models for the Central and Eastern North America Region, PEER Report Number 2015/04*, University of California, Berkeley, California, 85–118.

Yenier, E., and G. M. Atkinson (2015b). An equivalent point-source model for stochastic simulation of earthquake ground motions in California, *Bull. Seismol. Soc. Am.* **105,** 1435–1455.

Yong, A., A. Martin, K. Stokoe, and J. Diehl (2013). ARRA-funded V_{S30} measurements using multi-technique approach at strong-motion stations in California and central-eastern United States, *U.S. Geol. Surv. Open-File Rept. 2013–1102*, 65 pp.

U.S. Geological Survey
345 Middlefield Road
Menlo Park, California 94025
boore@usgs.gov
(D.M.B.)

CoreLogic, Inc.
555 12th Street, Suite 1100
Oakland, California 94607
kcampbell@corelogic.com
(K.W.C.)

Manuscript received 30 June 2016;
Published Online 20 December 2016